

STM Image Simulations of Atomic Clusters and One-atom Switch

J.P. VIGNERON

Institute for Studies in Interface Sciences,
Facultés Universitaires Notre-Dame de la Paix
Rue de Bruxelles, 61, B-5000 Namur, Belgium.

Abstract. This paper describes the results of several scanning tunnelling microscope (STM) computer simulations. In these simulations, a model tungsten tip is used to scan adsorbed clusters of xenon atoms lying on a clean surface of nickel. The computer program views the tip and the adsorbate as discrete atomic clusters attached to the planar surface of facing Sommerfeld metallic half spaces. The potential barrier crossed by the tunnelling electron is constructed from the measured values of the tip and substrate work functions and Fermi energies, supplemented by the effect of multiple electron images. The xenon and tungsten free-atom electronic structures are used to define the one-electron atomic pseudopotentials which create the three-dimensional scattering channels. It is shown that the detailed description of the elastic electron scattering on this three-dimensional potential barrier provides a quantitative description of the xenon images : (1) a single Xe atom, (2) a row of three Xe atoms and (3) the recently described one-atom switch.

1. Introduction

One of the clearest and best reproducible adsorbate system depicted by scanning tunnelling microscopes is the isolated xenon atom lying on a clean metal surface. Xe on Ni (110) also provides the attendant parts for the first one-atom switch¹.

There is something astonishing in the fact that the Xe atom appears so clearly in STM images in view of the low value of the adsorbed Xe density of states at the tunnelling energy. This problem was examined by Eigler *et al.*¹ who showed that the shape and corrugation of the constant-current tunnelling signal appear compatible with an atom-on-jellium model of the local density of states of the adsorbate. This description of the STM image neglects the tip-sample interaction and requires a significant adsorption-induced broadening of the *s* and *p* states of xenon to provide enough contribution to the local density of states at the tunnelling energy. This broadening is however quite difficult to assess, in part because the adsorption distance of Xe on Ni is known to be rather large (close to 3 Å above the centre of the first-layer Ni atoms) and because the binding is highly dependent on intricate correlation effects, still difficult to describe with highly localised electron densities.

On the other hand, we note the presence of a 5 *d* state of tungsten relatively close to the tunnelling energy. The importance of a *d* state pointing out of the tip apex has been properly recognised by Chen² as a factor of improvement for resolution and sensitivity in many STM experiments. The description of the image in terms of the Xe-induced changes in the sole local surface density of states of nickel may not be satisfactory and leads us to consider an extended approach, with a more symmetrical treatment of the tip and the sample, and more emphasis on the electronic interaction between them.

2. Methodology

A reliable description of the tunnelling process taking place in the STM starts with a careful description of the different contributions to the potential energy, and is followed by a very accurate

representation of the associated scattered carrier wave functions. Such a scheme, which improves on many computations based on the Bardeen transfer hamiltonian and approximate models of the tip and sample wave functions^{3, 4, 5, 6} has been introduced by Lucas *et al.*^{7, 8} in the framework of a Green function formalism. Similar ideas have later been applied to more refined STM models⁹, or extended to exhibit a more detailed information about the electron flow^{10, 11}. A preliminary account of the basic ideas sustaining the transfer-matrix approach used in the present paper can be found in a short paper by Derycke *et al.*¹² and this will only be summarised here. Standard semi-empirical quantum chemistry is now able to provide input to highly sophisticated and convincing STM simulations¹³, including the case of adsorbate imaging¹⁴.

The region where the scattering takes place is the gap which separates the planar surfaces of two free-electron metals. The first metal (*I*) carries the tip cluster and the second metal (*III*) carries the adsorbate. The free-electron metals are each described by two parameters, the experimental work functions Φ_S (sample side) and Φ_T (tip side) (in the range 4-5 eV) and the bulk Fermi levels E_{FS} and E_{FT} (in the range 10-20 eV). At equilibrium (vanishing external bias V), the chemical potential (Fermi level, at low temperature) is constant, so the barrier between the planar metals exhibits a trapezoidal shape, with the top slightly tilted by the contact electric field arising from the difference in work functions. This trapezoidal barrier is further modified by the multiple image potential arising from the dynamic charge induced on both metal surfaces¹⁵. Imbedded in this one-dimensional barrier, we find the three-dimensional forces on electrons induced by the presence of the tip apex and, on the other side, the adsorbate. These potential wells will be replaced by one-electron pseudopotentials, reduced to a local approximation, and fitted to gaussian functions for analytical convenience.

The transfer-matrix approach of the tunnelling current computation is basically borrowed from the dynamic low-energy electron diffraction theory¹⁶. In this approach, the incident waves are described as two-dimensional Bloch waves, which can be expanded into two-dimensional Fourier series, leading to the so-called Laue (or g - z) representation. In this representation, the wave vector \mathbf{k} is naturally split into a Brillouin-zone vector \mathbf{q} and a supercell reciprocal lattice vector \mathbf{g} :

$$\Psi_{(\mathbf{q}, \mathbf{g})}(\mathbf{r}) = \sum_{\mathbf{g}'} \phi_{\mathbf{g}\mathbf{g}'}^{(\mathbf{q})}(z) e^{i(\mathbf{q}+\mathbf{g})\cdot\mathbf{p}} \quad (1)$$

In this formalism, the Schrödinger equation is then a linear system of complex ordinary differential equations which, if solved with the appropriate boundary conditions, provides the dynamic (i.e. multiply-scattered) wave functions needed to compute the current.

In the tip and the sample substrates, the potential keeps a constant value (V_T on the tip side, and V_S on the sample side) and the general solution of the wave equation can be written in terms of one-dimensional travelling or evanescent sine waves. In the tip holder region (region *I*, $z < z_I$), we have

$$\sqrt{\Omega} \phi_{\mathbf{g}\mathbf{g}'}^{(\mathbf{q})}(z) = a_{\mathbf{g}'\mathbf{g}I}^+ e^{ik_{\mathbf{g}'I}(z-z_I)} + a_{\mathbf{g}'\mathbf{g}I}^- e^{-ik_{\mathbf{g}'I}(z-z_I)} \quad (2)$$

where Ω is the plane wave normalisation volume, and where the z -component (of positive real part) of the wave vector is given by

$$k_{\mathbf{g}'I} = \sqrt{\frac{2m(E - V_T)}{\hbar^2} - |\mathbf{q} + \mathbf{g}'|^2} \quad (3)$$

Similar expressions hold in the sample substrate region (region *III*, $z > z_{III}$). The search for the amplitudes $a_{\mathbf{g}'\mathbf{g}I}^+$ and $a_{\mathbf{g}'\mathbf{g}I}^-$ can be easily reduced, by linearity, to the integration of the one-dimensional system of Schrödinger equations, with *initial conditions* imposed at one edge of the

tunnelling barrier. The total current exiting a supercell can be computed by summing the contributions of all incident waves originating with energies between E_{FT} (tip Fermi level) and $E_{\text{FT}} - eV$ (for a bias V). This leaves us with the following expression, specialised to the case of a zero-bias conductance

$$e \frac{\partial I}{\partial V} = 2 \frac{e^2}{h} \frac{\sigma}{4\pi^2} \int_{\text{ZB}} d\mathbf{q}^2 \sum_{\mathbf{g}} \Theta(k_{\mathbf{g}\uparrow}^2(E_{\text{FT}})) \left[1 - \sum_{\mathbf{g}'} \frac{k_{\mathbf{g}\uparrow}(E_{\text{FT}})}{k_{\mathbf{g}'\uparrow}(E_{\text{FT}})} |a_{\mathbf{g}\mathbf{g}'}^-|^2 \Theta(k_{\mathbf{g}\uparrow}^2(E_{\text{FT}})) \right] \quad (4)$$

$e^2/h = 1/25813 \Omega^{-1}$ is the quantum Hall conductance.

We use this formula, including the reference current subtraction, in simulations where specific models have been designed to describe the scattering of electrons on the apex of a tungsten tip, while scanning a single Xe atom, a group of three Xe atoms properly aligned on a (110) Ni surface or a Xe atom switching in or out of a kink site. Our STM images can be explained in terms of the tip, adsorbate and substrate electronic structure interactions and, in particular, be put in relation with the changes of the scattered electron distribution as the tip position varies. These results show that the three-dimensional elastic electron scattering gives a convincing representation of the STM images of physisorbed Xe atoms^{17, 18}. In view of these results, it seemed relatively safe to undertake, with the same potential parameters, a study of the current contrast in the two-terminals single-atom switch.

3. The two-terminals one-atom switch

The two-terminals single-atom switch described by Eigler *et al.*¹ is a simple device directly derived from manipulations of Xe atoms on the surface of Ni. Here, however, the surface is chosen to be vicinal of (110) and a high-co-ordination site at a kink is used to stabilise the Xe atom. The tip of the STM is used to visualise the adsorbed atom and this information allows to bring the tip apex at an adequate distance to the Xe atom. In this position, using pulses of tunnel current, the Xe atom can be reversibly moved from its kink site to an adsorption site on the tip. Little is known on this tip adsorption site and we cannot know very precisely from experiment if the tip experiences any geometric rearrangement due to the Xe capture. The motion of the Xe atom induces reproducible changes in the conductivity of the tunnel junction, which define two distinct states: the "on" state of high-conductance obtained when the Xe atom is captured by the tip and the "off" state of low conductance obtained when the Xe lies on the Ni surface. The current contrast between the "on" and "off" states is found to be close to 7 with an initial (low-conduction) resistance of 1.6 M Ω .

In order to represent the kink site, an incomplete layer of Ni atoms is constructed above the planar "Sommerfeld" Ni surface (9.3 eV Fermi level and 4.9 eV work function). A gaussian pseudopotential (1.4 Å radius, 14.2 eV depth) is used to define an array of wells which covers half the supercell plus a further half row. The parameters for the wells are chosen to produce a "natural extension" (with the same mean potential energy) of the Sommerfeld metal representing Ni. The kink site is located at the termination of the extra half row. The macroscopic single-atom-tip-holder, considered to be tungsten, is also modelled by a Sommerfeld metal surface described by a Fermi level 19.1 eV above the constant effective potential V_{T} and a work function of 4.6 eV. The tungsten apex atom is modelled by a sum of gaussian pseudopotential wells (1.56 Å radius, 23.7 eV depth) with strengths adjusted to bring a d state at the self-consistent $5d$ atom-level (-6.0 eV) and a s state at the $6s$ atom level (-7.0 eV). The centre of this well is placed at the adsorption distance of 0.8 Å (measured from the centre of the W adatom to the edge of its supporting Sommerfeld metal). The Xe potential is chosen to bring the p state close to -7.5 eV and the s state within 1 eV below the vacuum level. These are the values suggested by a self-consistent relativistic calculation of the free atom, for a configuration $(\text{Xe}^-)_j$ where the $6s$ state is entirely occupied. Following the experimental procedure, the tip apex is not placed straight above the Xe atom, but displaced laterally, above the terrace, by an amount of 5 Å (this is important to improve on the chances that the Xe returns to the kink site in a "switch off" transition).

In the experiment of Eigler *et al.*¹, the "off" state resistance is 1.5 M Ω . In the present simulation,

with the Xe adsorbed at the kink site, the distance s between the tip and the sample Sommerfeld edges is adjusted to a value of 7.36 \AA , which gives a centre-to-centre distance from the apex W atom to the adsorbed Xe atom of 7 \AA (which represents a tip apex 5 \AA above the lower terrace, and 3.8 \AA above the upper terrace), as suggested in the report of Eigler *et al.*¹. The result of the evaluation of the tunnel resistance in that case gives the very satisfactory value $G = 1.6 \text{ M}\Omega$, which provides a confirmation, *a posteriori*, of the top-sample distance suggested in the experimental report.

We now proceed to study the conductance of the "on" state. The Xe atom is then on the tip, presumably still close to the apex, as it seems to keep ready to return to the kink site as soon as the "off" pulse is applied. The structure of the tip apex is not precisely known and we should make reasonable guesses about the geometry of the terminating tungsten cluster and the location of the Xe adsorption site. Since a BCC crystal has a lower surface energy on a (110) surface, we assume a $\langle 111 \rangle$ or $\langle 100 \rangle$ oriented tip terminated by a pyramid-shaped apex with four orthogonal facets. Each facet is then a triangular portion of (110) surface and, here again, we are entitled to consider several possibilities of adsorption sites for Xe. Even if locally symmetric sites of co-ordination 1, 2 or 3 can be found on this undistorted tungsten tip, we should expect that the tip rearrangement under a Xe capture invalidates any symmetry-based assessment of the adsorption configuration. The geometries specifically studied in this work are described in Fig. 1. In all parts of this figure, the tip apex kept at the same distance from the nickel terraces ($s = 7.36 \text{ \AA}$). Part (a) of Fig. 1 describes the low conduction state which provides a tunnel resistance of $1.6 \text{ M}\Omega$. Part (b) of Fig. 1 shows the simulation of the tunnelling in the (naive) highly symmetric configuration where the Xe atom hangs "on top" of the tip apex. This geometry provides a maximum lowering of the tunnel barrier and yields a resistance 66 times smaller than in the "off" state ($0.025 \text{ M}\Omega$). In part (c) of Fig. 1, the Xe atom is supposed to be adsorbed on the 3-fold co-ordinated hollow site on the side of the W pyramid, lying slightly (0.4 \AA) lower than the apex W atom. In this configuration the potential barrier is nearly as wide as in the "off" state and the current is only enhanced by a factor 3.9 ($0.42 \text{ M}\Omega$). The conductance enhancement is here partly due to the fact that the Xe atom effectively doubles the tunnelling channel width. The experimental enhancement (a factor 7) is somewhere between these two extreme positions of the Xe atom, most probably closer to the geometry described by Fig. 1 (c). A slight relaxation of the tip bringing the Xe at a larger distance of the tip holder surface could easily lead to a much better value of the conductance contrast. However, due to many uncertainties in the structure of the undistorted tip, we think we have reached here a limit for the predictive power of our model and we then refrain from making a stronger statement about the involved relaxation. Finally, as a last indication on the possible influence of the Xe rearrangement on the tip apex, we like to mention the series of results summarised on Fig. 2, where the Xe atom is considered to occupy the same site as in Fig. 1 (c), but for the four different faces of the pyramid of tungsten atoms at the tip apex, and for a second position of the tip relative to the kink site. We note that the resistance ranges from $0.13 \text{ M}\Omega$ to $0.19 \text{ M}\Omega$, which means that we do not observe a drastically different conductance when the Xe atom is considered to move around the tip apex.

4. Summary and conclusions

First, this paper has introduced a new, highly accurate procedure. We have shown that the procedure used to compute the tunnel conductance of a STM is efficient enough to produce simulated images in all modes of operation of the STM (constant-height, constant current or effective barrier height mode). The basic idea sustaining this theory is that tunnelling, including part of the electronic tip-sample interaction (without carrying out self consistency), can be treated as a three-dimensional scattering problem in a one-body context, with potential barriers based on the knowledge of surface work functions, perturbed by multiple image effects. The method has been applied to simulations allowing to compare the case of Xe adsorption "on top" and in the "hollow" high-co-ordination site. Our results favour the "on top" configuration, a result which suggests that the Xe/Ni bonding contains more than a simple Van der Waals effect. This result was already suggested by Joachim and Eigler in recent analysis of STM scans showing the stripe-shaped corrugation of the Ni (110) surface as a background

to the Xe image¹⁹.

The study of the two-terminals one-atom switch is somewhat more complicated, but involves the same theoretical ingredients. In the simulations described here, the low and high conduction states are properly recognised, and the current contrast between those states is found with the correct order of magnitude (a value between one and ten). This simulation calls for a better knowledge of the adsorption site of Xe on the tip apex in this experiment and of the relaxation which might rearrange the atoms when the Xe is captured. Such a study is outside the scope of the present paper. Further imaging experiments on various simple ad atoms with a tip carrying a xenon atom might be of further help, while self consistent quantum-chemistry calculations of Xe on tungsten clusters should be advocated to give preliminary informations on this subject.

Acknowledgements

We are grateful to K. Kambe, M. Scheffler, G. Doyen, D. Drakova and D. Eigler for discussions and many comments and suggestions during the development of this work. Part of this article presents research results of the Belgian Program of Interuniversity Attraction Poles initiated by the Belgian State-Prime Ministers Office-Science Policy Programming. The work was also partly funded by the Belgian national program of Interuniversity Research Projects initiated by the State-Prime Minister Office (Science Policy Programming): project ELSAM (Electronic Large Scale Computational System for Advanced Materials). We acknowledge the use of Namur Scientific Computing Facility (Namur-SCF), a common project between FNRS, IBM Belgium, and the Facultés Universitaires Notre-Dame de la Paix (FUNDP).

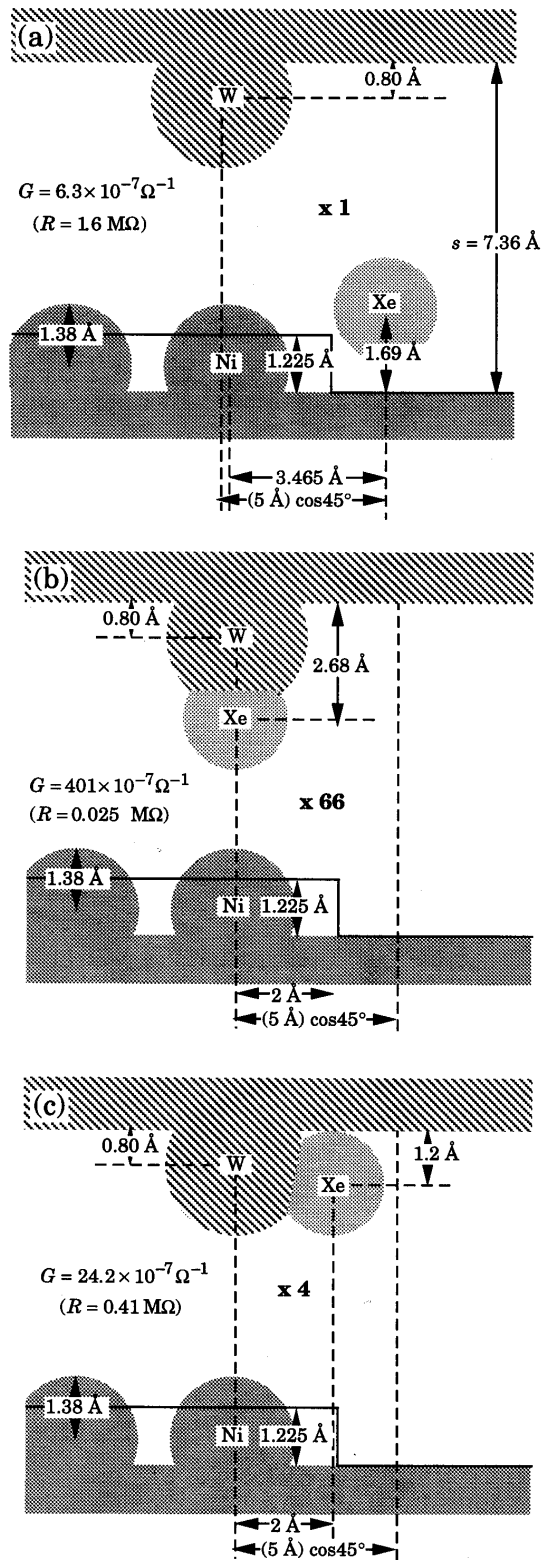


Figure 1. Three simulations describing the operation of the two-terminals one-atom switch based on Xe/Ni (110). (a) The low-conductance state, with a resistance of $R_T = 1.6 \text{ M}\Omega$; (b) The "on top" model, for which a resistance of $R_T/66$ is found; (c) the (seemingly more probable) "hollow-site" model, with a resistance of $R_T/4$.

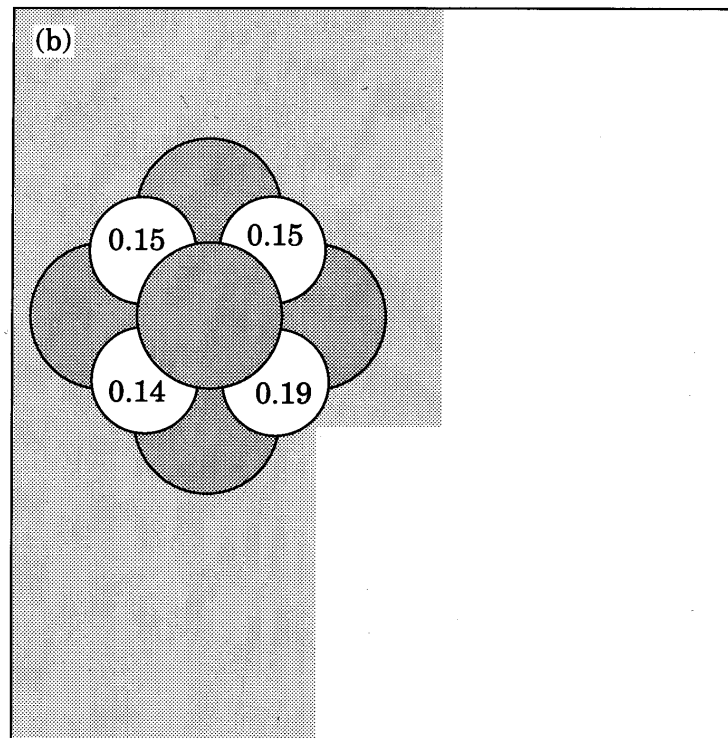
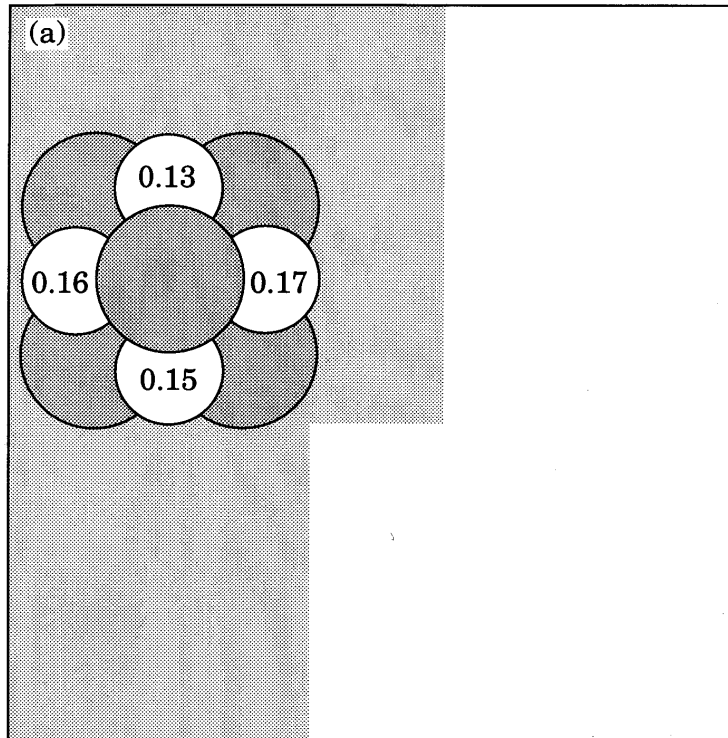


Figure 2. Tunnel resistances (in $M\Omega$) found for different orientations of the tungsten-xenon bonds around the tip apex. The resistance is not drastically changed by the choice of the orientation.

References

- ¹ Eigler D.M., Weiss P.S., Schweizer E.K., and Lang N.D., Phys. Rev. Letters **66**, 1189-1192 (1991)
- ² Chen C.J., J. Vac. Sci. Technol. A **6**, 319-322 (1988)
- ³ Lang N.D., Phys. Rev. Lett. **55**, 230-233 (1985); erratum: **55**, 2925 (1985), and Lang N.D., Phys. Rev. Lett. **56**, 1164-1167 (1986)
- ⁴ Selloni A., Carnevali P., Tosatti E. and Chen C.D., Phys. Rev. B **31**, 2602-2605 (1985); erratum : Phys. Rev. B **34**, 7406 (1986)
- ⁵ Chung M.S., Feuchtwang T.E. and Cutler P.H., Surface Sci. **187**, 559-568 (1987)
- ⁶ Leavens C.R. and Aerts G.C., Phys. Rev. B **38**, 7357-7364 (1988)
- ⁷ Lucas A.A., Morawitz H., Henry G.R., Vigneron J.P., Lambin Ph., Cutler P.H. and Feuchtwang T.E., Phys. Rev. **37**, 10708-10720 (1988)
- ⁸ Lucas A.A., Morawitz H., Henry G.R., Vigneron J.P., Lambin Ph., Cutler P.H. and Feuchtwang T.E., J. Vac. Sci. Technol. A **6**, 296-299 (1988)
- ⁹ Doyen G., Koetter E, Vigneron J.P. and Scheffler M., Appl. Phys. A **51**, 281-288 (1990)
- ¹⁰ Laloyaux Th., Lucas A.A., Vigneron, J.P., Lambin Ph., and Morawitz H., J. Microsc. **152**, 53-63 (1988); Laloyaux Th., Derycke I., Vigneron J.P., Lucas A.A., Phys. Rev. B **47**, 7508-7518 (1993)
- ¹¹ Lucas A.A., Europhys. News **21** (1990)
- ¹² Derycke I., Vigneron J.P., Lambin Ph., Laloyaux Th. and Lucas A.A., Quantum Chemistry Symposium **25**, 687-702 (1991)
- ¹³ Sautet Ph. and Joachim C., Ultramicroscopy 42-45, 115 (1992); Sautet Ph. and Joachim C., Surf. Sci **271**, 387 (1992)
- ¹⁴ We acknowlegde receipt of publications in preprint form from Bouju and Joachim (Phys. Rev.), Girard and Joachim (Surf. Sci.), Joachim and Sautet (Europhysics Lett.)
- ¹⁵ Lucas A.A., Vigneron, J.P., Bono J., Cutler P.H., Feuchtwang T.E., Good R.H.Jr. and Huang Z., J. Phys. Colloid Chem. C **9**, 125 (1984)
- ¹⁶ Pendry J.B., in "Low Energy Electron Diffraction" Academic Press, London (1974)
- ¹⁷ Vigneron J.P. and Derycke I., J. Vac. Sci. Technol. B **12**, 2161 (1994)
- ¹⁸ Vigneron J.P., Derycke I., Laloyaux Th., Lambin Ph., Lucas A.A., Scanning Microscopy Suppl. 7, Proceedings of the 11th Pfefferkorn Conference, Amherst 1992
- ¹⁹ Joachim, C. and Eigler, D., private communication.